

## LETTERS

# Field evidence for surface-wave-induced instability of sand dunes

Hicham Elbelrhiti<sup>1,2</sup>, Philippe Claudin<sup>1</sup> & Bruno Andreotti<sup>1</sup>

**Field studies of barchans—crescent-shaped dunes that propagate over solid ground under conditions of unidirectional wind<sup>1</sup>—have long focused on the investigation of an equilibrium between sand transport by wind and the control of air flow by dune topography<sup>2–4</sup>, which are thought to control dune morphology and kinematics<sup>5–7</sup>. Because of the long timescale involved, however, the underlying dynamic processes responsible for the evolution of dune fields remain poorly understood<sup>8</sup>. Here we combine data from a three-year field study in the Moroccan Sahara with a model study to show that barchans are fundamentally unstable and do not necessarily behave like stable solitary waves, as suggested previously<sup>9–12</sup>. We find that dune collisions and changes in wind direction destabilize the dunes and generate surface waves on the barchans. Because the resulting surface waves propagate at a higher speed than the dunes themselves, they can produce a series of new barchans of elementary size by breaking the horns of large dunes. The creation of these new dunes provides a mechanism for sand loss that prevents dune fields from merging into a single giant dune and therefore plays a fundamental role in the control of size selection and the development of dune patterns.**

Very few barchans in a dune field exhibit the smooth crescent shapes that are simulated in models (Fig. 1e); instead they display more complex substructures. The windward slope and flanks of barchans generally present superimposed bed-forms which can become high enough to induce air-flow separation and thus secondary avalanche slip faces (Fig. 1b–d). On the basis of the numerical findings that two colliding barchans can cross through one another while still preserving their shape, these phenomena have been interpreted as small dunes climbing onto large ones<sup>9–11</sup>. This is contradicted by our direct field investigation, during which we have followed the birth, growth, propagation and further evolution of these structures. We studied more than a hundred barchans in the region between Tarfaya (27° 56' N, –12° 56' W), Sidi Aghfinir (28° 06' N, –12° 03' W) and Lâayoune (27° 10' N, –13° 14' W), where the wind regime (wind rose on Fig. 1) is one of the most unimodal<sup>13</sup>. Two situations under which the dune surface becomes destabilized are identified: changes of wind direction (Fig. 1a–d) and collisions (Fig. 1f–i). We have precisely investigated the detailed nature of the unstable modes on five dunes displaying well-defined patterns. With the help of fixed markers, we observed that the undulations propagate downwind on the stoss (windward) slope and the flanks of the dune at a velocity  $c \approx 2 \text{ m day}^{-1}$ , which is typically ten times larger than that of the dune itself. Their wavelength and amplitude do not vary much in the course of their motion. We have measured the variations of height  $\delta h$  and sand flux  $\delta q$  on a cut line along a barchan horn (Fig. 2b). These quantities are proportional, which demonstrates that these undulations behave as plane propagating waves.

The nucleation and propagation of such waves on a sand bed is governed by the interaction between the bed profile, which modifies the air flow, and the sand transport, which controls the erosion and deposition processes. Along the upwind side of a hump, the streamlines converge, yielding an increasing wind and thus an increasing flux, so that erosion takes place<sup>2–4</sup>. Conversely, the flux decreases on the downwind side causing accretion, which in total means that the bump translates downwind. However, the accretion does not start precisely at the crest but is shifted upwind, so that the bump is amplified. This instability mechanism is directly related to the asymmetry of the wind flow, which originates in the nonlinear inertial term of the Navier–Stokes equations. So far in this description, no length scale is involved, because the atmospheric boundary layer is fully turbulent, and the mechanism therefore predicts an unconditional instability at all wavelengths. There is however a small-scale cut-off for the instability related to the transient approach to saturation of the sand flux. As exemplified in Fig. 3b, the flux reaches its equilibrium value, determined by the wind strength, over a characteristic distance  $L$  called the saturation length. This effect shifts downwind the position at which the flux  $q$  is maximum, and thus stabilizes small bumps.

Previously<sup>8</sup>, we have derived a simple model (called<sup>8</sup>  $C_C^2$ ) accounting for all the above mechanisms: mass conservation, shape-flux coupling and flux saturation. Here we present field measurements of the quantities characterizing the unstable waves—wavelength, propagation speed and amplitude—and quantitatively compare them to the predictions of the model. Three dimensionless parameters  $A$ ,  $B$  and  $D$  enter the model, which respectively govern the wind acceleration on a bump, the displacement upwind of the maximum velocity and the lateral coupling. Their values are tuned to reproduce the relations between the morphological parameters of barchans: height, width and length (Fig. 1e). The only timescale of the problem is related to the saturated flux  $Q$  on a flat bed and encodes the wind strength (wind roses on Fig. 1). The only characteristic length scale<sup>14</sup> is the saturation length  $L$  introduced above, and we designed a specific experiment to measure it on a 20-m-long and 3-m-wide flat sand sheet prepared with a bulldozer (Fig. 3b).  $L$  is directly related to the length needed for a grain to reach the wind velocity, which scales<sup>15</sup> with the grain density to fluid density ratio times the grain diameter  $d$ . Using the measured values  $L = 1.7 \text{ m}$  and  $d = 180 \mu\text{m}$ , we obtain:

$$L \approx 4 \frac{\rho_{\text{sand}}}{\rho_{\text{air}}} d \quad (1)$$

in close agreement with our re-analysis of Bagnold's experiment<sup>1</sup> ( $L = 2.3 \text{ m}$  for  $d = 250 \mu\text{m}$ ).

To derive the dispersion relation of surface waves, we have examined large dunes for which the scale separation is sufficient for us to consider that they are flat at the scale of the waves. In the

<sup>1</sup>Laboratoire de Physique et Mécanique des Milieux Hétérogènes (LPMHM), UMR CNRS 7636, 10 rue Vauquelin 75005 Paris, France. <sup>2</sup>Geology Department, Université Ibn Zohr, BP 28/5, Cité Dakhla, 80000 Agadir, Morocco.

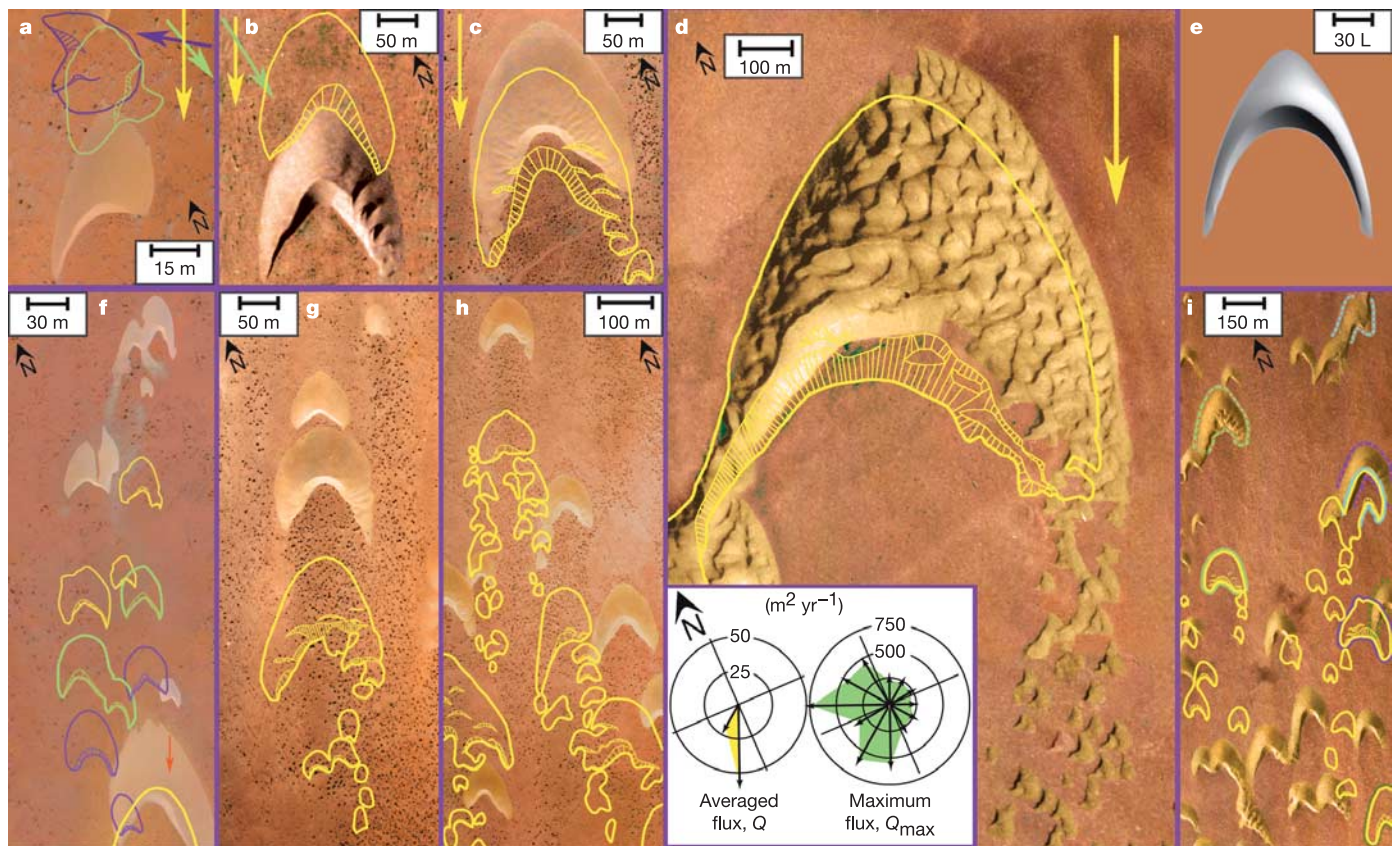


**Figure 1 | Response of barchan dunes to changes of wind direction and to collisions.** Coloured contours extracted from GPS data are superimposed to aerial photographs taken from a plane or a kite (Supplementary Information). The averaged sand flux rose (1999,  $Q = 80 \text{ m}^2 \text{ yr}^{-1}$ ) shows a narrow unimodal regime whose dominant direction, indicated by yellow arrows, is the average direction of barchan motion. The maximum sand flux rose reveals a more isotropic distribution of extreme events (Supplementary Information). **a–d**, Response of barchan dunes to changes of wind direction. **a**, Two profiles of a small dune (purple,  $t = -15$  months; green,  $t = -12$  months) superimposed on an aerial photograph ( $t = 0$ ). The slip face quickly readapts to changes of wind direction (corresponding arrows). **b**, Surface waves on a medium-sized dune, induced by a northwest wind (reference profile at  $t = -80$  months). **c**, Destabilization of a medium-sized dune leading to the emission of elementary barchans ( $t = 50$  months).

**d**, Mega-barchan ( $t = 350$  months). The surface waves are permanently driven by daily wind variations. **e**, Numerical dune produced by the  $C_C^C$  model<sup>8</sup>. The parameters ( $A = 8.4$ ,  $B = 8.0$ ,  $D = 0.4$ ) are tuned to get the same height, length and width as on **c**. **f–h**, Response of barchan dunes to collisions. **f**, Edging collisions between small dunes (yellow,  $t = 17$  months, green,  $t = 23$  months, purple,  $t = 33$  months). Note also a fusion (red arrow). **g**, Coaxial collision of medium-sized dunes leading to a larger dune with a wake of new elementary barchans ( $t = 60$  months). **h**, Chain destabilization of medium-sized dunes ( $t = 60$  months). The trail of a dune sustains the instability of the next one. **i**, Long-term ( $t = 350$  months) evolution of a barchan field. Even though the largest dunes (highlighted dashed contours) persist, many dunes appear or disappear, showing that dune destabilization is an essential process of large-scale rearrangement.

framework of the  $C_C^C$  model, the linear stability analysis of a uniform sand bed predicts an unconditional instability at large wavelengths of growth rate  $\sigma$  and propagation speed  $c$  given by:

$$\sigma = Qk^2 \left[ \frac{B - A|k|L}{1 + (kL)^2} - D \right] \quad c = \frac{Q|k|}{1 + (kL)^2} (A + B|k|L) \quad (2)$$

where  $k = 2\pi/\lambda$  is the mode wavenumber. As all modes propagate downwind, the instability is of convective type<sup>16</sup> so that the pattern develops spatially: any disturbance such as a change of wind direction or a colliding dune (Fig. 1) constitutes a seed amplified by the linear instability in the course of propagation.

The maximum growth rate—the most unstable mode predicted by equation (2)—is reached for a wavelength  $\lambda_{\text{max}} \approx 12L \approx 20 \text{ m}$ .  $\lambda$  was measured systematically in a zone of 500 regular barchans (1–12 m high). The histogram of these measurements, depicted on Fig. 3a, exhibits a clear peak around  $\lambda \approx 20 \text{ m}$ . The same measurements, performed on the windward side of the mega-barchan of Fig. 1d (40 m high), give a slightly larger wavelength of  $\lambda \approx 28 \text{ m}$ . This can be related to an increase of the wavelength—pattern coarsening—as the waves propagate, due to screenings and fusions. Situations where the fluid is much denser (water) or lighter (Mars

atmosphere) than air allows a further examination of the scaling proposed in equation (1). It gives the correct destabilization wavelength for submarine ripples in the turbulent case:  $\lambda_{\text{max}}$  reduces to a few centimetres, because water is 800 times denser than air. Martian dunes<sup>17</sup> present surface waves of wavelength around 600 m for an atmosphere 80 times lighter than Earth's. According to our analysis, the grains in saltation forming these dunes should have a diameter of  $75 \mu\text{m}$ , which corresponds to the size of the dominant species composing the aeolian ripples photographed by the Mars rover Opportunity<sup>18</sup>.

As shown in Fig. 2a, the velocity of large barchans decreases with height  $H$  following the Bagnold relation<sup>1</sup>  $c \approx aQ/H$ , where  $a \approx 2.7$  represents the increase in flux between the ground and the brink and is measured independently (Supplementary Information). Furthermore, we expect the velocity of barchans to match that of waves in the limit of vanishing amplitude, for which equation (2) predicts:  $c \approx c(\lambda_{\text{max}}) \approx 5.3Q/L$ . This suggests that we should modify the Bagnold relation:

$$c = aQ/(H + H_0) \quad (3)$$

where  $H_0 = aL/5.3 \approx 87 \text{ cm}$  is a cut-off that corresponds to the

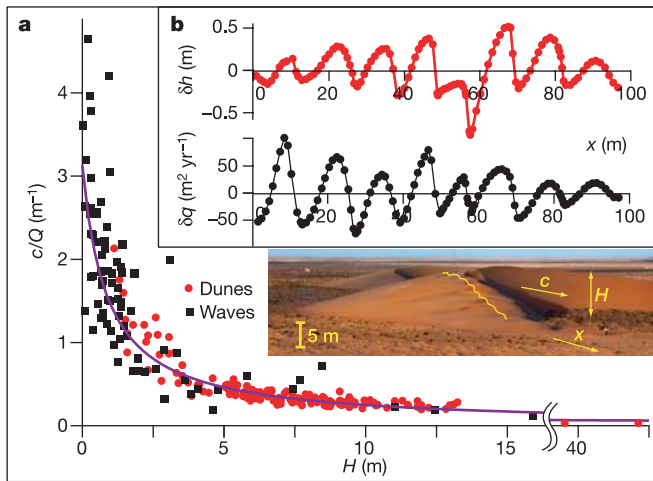


**Figure 2 | Wave-like behaviour of surface undulations.** **a**, Comparison of the velocity  $c$  of waves and dunes as a function of their height  $H$ . The velocity of 140 dunes is measured using several aerial photographs and global positioning system (GPS) data, with displacements resolved to within 4 m. The velocity is averaged over two time intervals (300 to 350 months and 10 to 18 months) to sample both large dunes that do not propagate much over a year, and small ones that cannot be followed over long periods of time (see Fig. 1i). The waves were marked with sticks and their displacements measured after a few hours. The corresponding velocities follow the same law as that of dunes, given a redefinition of  $Q$ : it is the saturated flux on solid ground averaged over the period of time considered in the case of dunes, and in the case of waves, the local saturated flux estimated from their altitude and from the propagation of neighbouring barchans (Supplementary Information). The purple solid line corresponds to the prediction of equation (3). **b**, Comparison of a wave profile  $\delta h$  with the corresponding modulations of sand flux  $\delta q$ . Sticks are placed regularly along a cut of a barchan horn (yellow line on the photograph). The slope and the distance between sticks allow for the reconstruction of the height profile  $\delta h$ .  $\delta q$  is derived from the erosion rate  $\partial_t h$ , using mass conservation:  $\delta q = -\int \partial_t h dx$  (Supplementary Information). The oscillations of  $\delta q$  in phase with those of  $\delta h$  are characteristic of a plane propagating wave  $h(x - ct)$  for which  $\delta q = \int c \partial_x h dx = c \delta h$ . The local wave velocity  $c = \delta q / \delta h$  decreases down-slope, like the local flux  $Q$ .

minimal barchan height. Field data (Fig. 2a) shows a quantitative agreement with this model equation for the slow motion of barchans on solid ground, but also for the fast motion of waves on the surface of dunes. It demonstrates that large-amplitude waves behave as barchans.

As for any convective instability, the amplitude of the waves depends on the amplitude of the disturbances applied to the dune, as well as on the length of the dune itself. This is well illustrated by the response of dunes to changes of wind direction. The medium-sized dune of Fig. 1c can remain almost undisturbed because it is sufficiently isolated and the wind sufficiently constant. Whereas dunes of size  $\lambda_{\max}$  are small enough to quickly readapt their shape (Fig. 1a), larger ones ( $\sim 5\text{--}10\lambda_{\max}$ ) generate a certain number of waveforms in the lee flank (Fig. 1b, c). The mega-barchan of Fig. 1d is so large ( $30\lambda_{\max}$ ) that the daily wind variations ( $\sim 15^\circ$ ) render its surface permanently unstable. Barchans and mega-barchans thus belong to the same class of dunes, the corrugations resulting from a size effect. A colliding dune constitutes another type of perturbation. Figure 1g shows a typical example of coaxial collision between two large dunes ( $3.5\lambda_{\max}$  and  $6\lambda_{\max}$ ), one catching the other up from behind. Displaying behaviour that is far from soliton-like (solitons are propagative solitary waves which do not interact with each other), the impacting dune induces large-amplitude waves on the flanks of the target dune, which amplify in the course of their propagation.

Figure 1i shows that these waves not only decorate the dunes, but

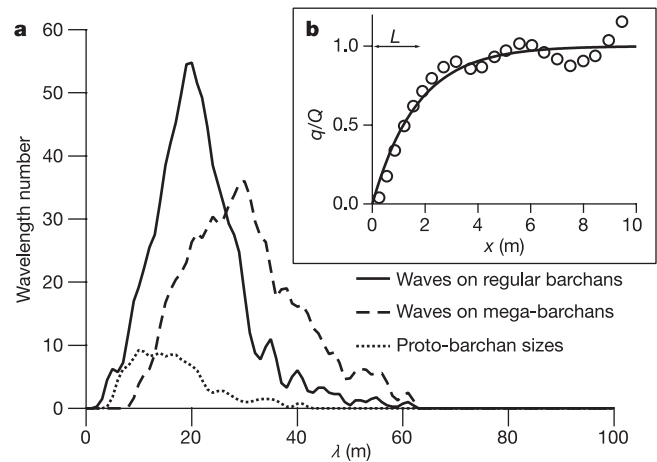


**Figure 3 | Wavelength distribution and saturation length.** **a**, Histograms of the wavelength  $\lambda$  measured systematically in a zone of 20 km  $\times$  8 km (solid line, 930 data points), as well as on the windward side of the mega-dune shown on Fig. 1d (dashed line, 850 data points), using 1-m bins. The peak of the distribution is reached for  $\lambda = 20$  and 28 m respectively, which is consistent with the linear stability analysis. The histogram of the length of proto-barchans—dome dunes without slip face—is also superimposed (dotted line, 160 data points). It shows a peak at 14 m. **b**, Spatial transient of sand transport saturation. A 20-m-long sand sheet is prepared with a bulldozer on the solid ground and protected to insure a null flux at the upwind edge. As for the wave profiles (Fig. 2b), the flux is measured by integrating the erosion rate  $\partial_t h$ , averaged over 24 h. The data are well fitted by an exponential relaxation  $q = Q[1 - \exp(-x/L)]$ , which corresponds to a first-order equation of saturation,  $L\partial_x q = Q - q$ .

play a crucial part in the long-term evolution of a barchan field. When a wave reaches solid ground at the end of the horn, an elementary dune of typical size slightly smaller than  $\lambda_{\max}$  (Fig. 3a) is detached and emitted. Globally, this produces numerous newborn dunes in the wake of the collision and thus a large sand loss from the procreative dunes. There are only two circumstances under which this collision mechanism apparently looks like a non-interactive process (1) the case where the two interacting dunes are themselves of lengths comparable to the elementary size  $\lambda_{\max}$  and (2) the case where they only brush against each other (Fig. 1f). We have demonstrated<sup>8</sup> that dunes behaving as stable kinematic waves would not lead to the size selection observed in barchan fields. On the contrary, the whole dune field would merge into a single giant dune. To resolve this problem, there should exist a sand leak increasing with the dune size: our field study shows that the induction of waves on the surface of dunes, breaking the horns into elementary barchans, provides this missing mechanism.

Received 18 December 2004; accepted 30 June 2005.

- Bagnold, R. A. *The Physics of Blown Sand and Desert Dunes* (Methuen, London, 1941).
- Wiggs, G. F. S., Livingstone, I. & Warren, A. The role of streamline curvature in sand dune dynamics: evidence from field and wind tunnel measurements. *Geomorphology* **17**, 29–46 (1996).
- Lancaster, N., Nickling, W. G., McKenna-Neuman, C. K. & Wyatt, V. E. Sediment flux and airflow on the stoss slope of a barchan dune. *Geomorphology* **17**, 55–62 (1996).
- McKenna-Neuman, C., Lancaster, N. & Nickling, W. G. Relations between dune morphology, air flow, and sediment flux on reversing dunes, Silver Peak, Nevada. *Sedimentology* **44**, 1103–1113 (1997).
- Finkel, H. J. The barchans of southern Peru. *J. Geol.* **67**, 614–647 (1959).
- Hastenrath, S. L. The barchans of the Arequipa region, southern Peru. *Z. Geomorphol.* **11**, 300–331 (1967).
- Andreotti, B., Claudin, P. & Douady, S. Selection of dune shapes and velocities—Part 1: Dynamics of sand, wind and barchans. *Eur. Phys. J. B* **28**, 321–339 (2002).
- Hersen, P. et al. Corridors of barchan dunes: stability and size selection. *Phys. Rev. E* **69**, 011304 (2004).

9. Besler, H. Complex barchans in the Libyan Desert: dune traps or overtaking solitons? *Z. Geomorph. N.F. Suppl.-Bd.* **126**, 59–74 (2002).
10. Schwammle, V. & Herrmann, H. J. Solitary wave behaviour of sand dunes. *Nature* **426**, 619–620 (2003).
11. Katsuki, A., Nishimori, H., Endo, N. & Taniguchi, K. Collision dynamics of two barchan dunes simulated by a simple model. *J. Phys. Soc. Jpn* **74**, 538–541; preprint at (<http://arXiv.org/cond-mat/0403312>) (2005).
12. Livingstone, I., Wiggs, G. F. S. & Baddock, M. Barchan dunes: why they cannot be treated as solitons or solitary waves. *Earth Surf. Process. Landforms* **30**, 255–257 (2005).
13. Fryberger, S. G. & Dean, G. in *A Study of Global Sand Seas* (ed. McKee, E. D.) 137–169 (Geol. Surv. Prof. Pap. 1052, Washington, 1979).
14. Hersen, P., Douady, S. & Andreotti, B. Relevant length scale of barchan dunes. *Phys. Rev. Lett.* **89**, 264301 (2002).
15. Andreotti, B. A two-species model of aeolian sand transport. *J. Fluid Mech.* **510**, 47–70 (2004).
16. Huerre, P. & Monkewitz, P. P. Local and global instabilities in spatially developing flows. *Annu. Rev. Fluid Mech.* **22**, 473–537 (1990).
17. European Space Agency. *Mars Express* ([http://www.esa.int/SPECIALS/Mars\\_Express/](http://www.esa.int/SPECIALS/Mars_Express/)) (23 June 2005).
18. Mars Rover Blog. *Mars Rover Photos* (<http://www.markcarey.com/mars/mars-rover-photos.html>) (23 June 2005).

**Supplementary Information** is linked to the online version of the paper at [www.nature.com/nature](http://www.nature.com/nature).

**Acknowledgements** We thank H. Bellot and L. Quartier for assistance during field measurements, R. Hoyle, B. Murray and J. Snoeijer for critical reading of the manuscript, and H. Tsoar for the provision of sand roses. This study was supported by an ACI Jeunes Chercheurs.

**Author Information** Reprints and permissions information is available at [npg.nature.com/reprintsandpermissions](http://npg.nature.com/reprintsandpermissions). The authors declare no competing financial interests. Correspondence and requests for materials should be addressed to B.A. ([andreotti@pmmh.espci.fr](mailto:andreotti@pmmh.espci.fr)).